Journal of the Optical Society of America B
OPTICAL PHYSICS

Constraints on downconversion in atomically thick films

Loris Marini,[1,2,3,6] L. G. Helt,[4] Yuerui Lu,[5] Benjamin J. Eggleton,[1,2,3] and Stefano Palomba[1,2,3,*]

[1]Centre for Ultrahigh Bandwidth Devices for Optical Systems (CUDOS), Sydney, NSW 2006, Australia
[2]Institute of Photonics and Optical Science (IPOS), The University of Sydney, Sydney, NSW 2006, Australia
[3]Australian Institute for Nanoscale Science and Technology (AINST), University of Sydney, Sydney, NSW 2006, Australia
[4]Department of Physics, Engineering Physics and Astronomy, Queen's University, Kingston, ON K7L 3N6, Canada
[5]Australian National University, College of Engineering and Computer Science, Canberra, ACT 0200, Australia
[6]e-mail: loris.marini@sydney.edu.au
*Corresponding author: stefano.palomba@sydney.edu.au

Received 20 November 2017; revised 15 January 2018; accepted 23 January 2018; posted 25 January 2018 (Doc. ID 313660); published 6 March 2018

Spontaneous parametric downconversion (SPDC) has been predicted in atomically thick crystals, though not yet observed. In this work we uncover physical and experimental constraints of photon-pair generation in such planar nonlinear films with a free-space illumination/collection geometry. We measure the material nonlinear response of monolayer tungsten diselenide via second harmonic generation and subsequently calculate the expected SPDC efficiency from appropriate quantum-classical relations. Energy and momentum conservation shape the wavevectors of photon pairs in free-space and allow us to calculate the loss and coincidence-to-accidental ratio in various configurations. This work improves the understanding of the nonlinear quantum optical potential of these crystals, guides their experimental validation, and provides a performance benchmark for these ultrathin materials.

OCIS codes: (190.4350) Nonlinear optics at surfaces; (270.0270) Quantum optics; (190.4223) Nonlinear wave mixing; (190.4975) Parametric processes; (270.5290) Photon statistics; (320.7110) Ultrafast nonlinear optics.

https://doi.org/10.1364/JOSAB.35.000672

1. INTRODUCTION

Spontaneous parametric downconversion (SPDC) is the probabilistic conversion of an input photon into a pair of strongly correlated signal and idler photons. Predicted in 1967 and observed soon after in bulk crystals [1–3], it has since become a standard platform for entanglement generation and heralded single-photon sources [4,5]. A large number of SPDC integrated sources have been proposed and demonstrated over the years with small footprints, high brightness, and excellent purity of generated photon states. Examples include microtoroids [6,7] and integrated waveguides [8–12] with sizes fundamentally limited by diffraction. However, in these typical structures it can be difficult to independently engineer input and downconverted light dispersion relations to fulfill phase matching conditions, and linear and nonlinear optical properties are often linked as well, complicating device design and limiting device flexibility. On the contrary, highly subdiffraction sources of correlated photon pairs would be automatically phase-matched, inherently broadband, and decouple the optimization of intrinsic linear and nonlinear properties.

Monolayers of group IV transition metal dichalcogenides (TMDCs) are an interesting platform for subdiffraction photon pair generation thanks to their record-high intrinsic second order optical nonlinearity [13–19]. Moreover, heterostructures, mechanical strain [20–22], and electrostatic doping [23–25] have all been shown to offer a way to dynamically control bandgaps and nonlinear responses [26], which could enable low latency control of photon pair generation. In this paper we take a first step toward understanding the potential of TMDCs for nonlinear optical generation of photon pairs via SPDC. Our starting point is a TMDC monolayer as sketched in Fig. 1, where both illumination and collection occur in free space. We perform second harmonic generation (SHG) experiments and harness the correspondence between stimulated and spontaneous nonlinear optical interactions [27–35] to calculate the expected SPDC brightness. Our results include estimates of SPDC emission patterns as well as linear propagation and collection losses. We show that a pump at normal incidence leads to omnidirectional pair emission and a maximum pair collection probability. The small interaction volume limits the pair generation efficiency of our structure to be well below typical waveguide-based integrated sources and, as such, the observation of SPDC from a TMDC monolayer could prove

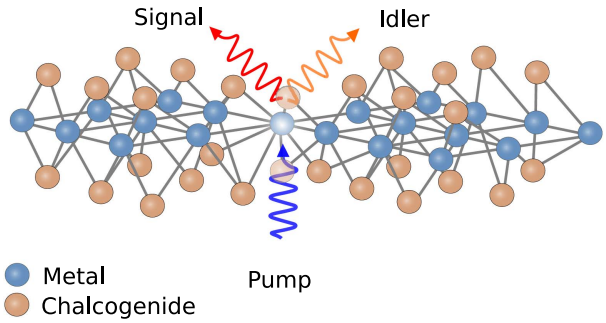

Fig. 1. SPDC from a monolayer of the TMDC WSe_2. A pump photon (blue) is incident from free space onto the nonlinear film and spontaneously converts into a signal (red) and an idler photon (orange).

challenging. However, we calculate that for dark-count limited measurements, the signal to noise ratio for such sources of photon pairs, known as the coincidence-to-accidental ratio (CAR) [36], could still be larger than 10. Our results pave the way to the experimental demonstration of localized SPDC in atomically thick films and provide a benchmark for the performance of other structures based on these materials.

2. QUANTUM CLASSICAL CORRESPONDENCE

SPDC is a quantum nonlinear process in which the zero-point vacuum field stimulates an input photon to transform into a pair of correlated photons. Energy and momentum must be conserved [37,38], and the probability that the process occurs depends quadratically on the medium second order susceptibility $\chi^{(2)}$.

The same conservation laws and scaling apply to the reverse (classical) process of SHG where two input photons give their sum energy to a single output photon. Although one process is quantum and the other classical, the efficiency of one can be estimated knowing the efficiency of the other [27,28,31–35]. While in general the effect of loss in the nonlinear medium has to be considered [29,30], here we neglect the loss since the material has an absorption coefficient of the order of $\alpha = 10^8$ m^{-1} [39] with a thickness of only $L = 0.7$ nm [26]. Furthermore, we approximate the TMDC monolayer as an incredibly short waveguide with a cross-sectional area equal to the diffraction-limited area of the pump beam (A_{SHG} or A_{SPDC} as appropriate).

Working in the undepleted pump approximation, we may write the photon flux generated in a perfectly phase-matched SHG experiment as

$$R_{\mathrm{SHG}} = \frac{\Delta t_{\mathrm{F}}}{T_{\mathrm{F}}} \frac{P_{\mathrm{F}}^2 L^2}{2\hbar\omega_{\mathrm{F}} \mathcal{P} A_{\mathrm{SHG}}}. \tag{1}$$

Here P_{F} is the peak power of the input pump at the fundamental frequency, Δt_{F} is the pulse width, T_{F} its repetition period, and

$$\mathcal{P} = \frac{8\varepsilon_0 n_{\mathrm{F}}^2 n_{\mathrm{SH}} c^3}{(\chi_{\mathrm{eff}}^{(2)})^2 \omega_{\mathrm{SH}}^2}, \tag{2}$$

which has units of power and contains quantities that depend on the nonlinear medium. Additionally the n_m are linear refractive indices at the fundamental ω_{F} and second-harmonic $\omega_{\mathrm{SH}} = 2\omega_{\mathrm{F}}$ frequencies, and $\chi_{\mathrm{eff}}^{(2)}$ is the effective material nonlinearity. Note that Eq. (1) is simply the usual quasi-continuous wave expression for generated SHG power [40] divided by the energy of an SHG photon, $2\hbar\omega_{\mathrm{F}}$, with the phase-matching term set to unity. As all optical interactions occur over a length much shorter than a wavelength, SHG in a TMDC monolayer is well approximated by this expression, even for subpicosecond pump pulses: the fields are phase matched, any group velocity mismatch leads to negligible walkoff, and dispersive pulse spreading can also be neglected.

Similarly, neglecting multipair generation, and in the undepleted pump approximation, the photon pair flux generated in a perfectly phase-matched SPDC experiment for an ultrathin waveguide can be written [27]

$$R_{\mathrm{SPDC}} = \frac{\Delta t_{\mathrm{P}}}{T_{\mathrm{P}}} \frac{\omega_{\mathrm{F}}}{3\pi} \frac{P_{\mathrm{P}} L^2}{\mathcal{P} A_{\mathrm{SPDC}}}, \tag{3}$$

where P_{P} is the peak power of the input pump at $2\omega_{\mathrm{F}}$ with duration Δt_{P} and repetition period T_{P}. Note that R_{SPDC} scales only linearly with pump power, whereas R_{SHG} scales quadratically. Additionally, because the process is always phase-matched, pairs are expected to be generated in a broadband continuum of modes around ω_{F} on the order of the inverse period of a generated photon $(3\pi/\omega_F)^{-1}$ [27]. We reserve consideration of non-energy-degenerate photon pair collection for future work. The ratio between the generation rates is

$$R_{\mathrm{SPDC}} = \frac{R_{\mathrm{SHG}}}{P_{\mathrm{F}}^2} \frac{\Delta t_{\mathrm{P}}}{\Delta t_{\mathrm{F}}} \frac{T_{\mathrm{F}}}{T_{\mathrm{P}}} \frac{2\hbar\omega_{\mathrm{F}}^2}{3\pi} \frac{A_{\mathrm{SHG}}}{A_{\mathrm{SPDC}}} P_{\mathrm{P}}, \tag{4}$$

and allows simple estimation of the rate of SPDC photon pair generation in a TMDC monolayer given a measurement of the rate of SHG photon generation in a different experiment with the same structure. Conveniently, this ratio does not depend on any material or structure parameters. In Fig. 2 we plot Eq. (3) for different $\chi_{\mathrm{eff}}^{(2)}$ and peak pump powers for the representative experimental values $\Delta t_{\mathrm{P}}/T_{\mathrm{P}} = 1.88\times10^{-5}$, $\omega_{\mathrm{SH}} = 2\pi \times 3.82 \times 10^{14}$ rad/s (785 nm wavelength), $A_{\mathrm{SPDC}} = 4.42\times10^{-13}$ m^2,

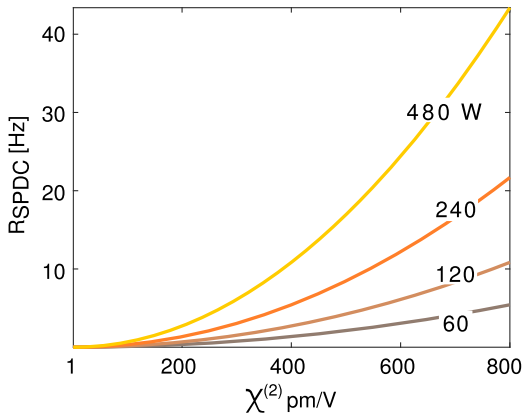

Fig. 2. Expected quadratic scaling of the rate of photon pairs generated via SPDC from a TMDC monolayer calculated using representative experimental values in Eq. (3), along with the linear refractive index of WSe_2 at the fundamental and second harmonic. Calculations show the expected linear scaling with pump peak power and assume illumination with an 80 MHz, 235 fs mode-locked pump.

and $L = 0.7$ nm, taking the relevant refractive indices to be $n_F = 4.0$ and $n_{SH} = 5.1$ [39]. Note that for SPDC, the pump is centered at ω_{SH} and photon pairs are collected near ω_F. This gives an initial picture of the possible rates of photon pair generation from individual monolayers of various TMDCs.

3. SPDC BRIGHTNESS FROM MONOLAYER WSe_2

Following our quantum-classical relations, a first step in obtaining an estimate of a potential SPDC generated photon pair flux is to measure the photon flux generated in an appropriate SHG experiment [recall Eq. (4)]. As a concrete example, here, and throughout the rest of this work, we focus on the specific TMDC of tungsten diselenide (WSe_2), which is known to exhibit strong light–matter interactions. In particular, the optical second-order nonlinearity of WSe_2 can be reversibly controlled by electrostatic doping [26], and its magnitude can be resonantly enhanced by up to a factor of 1000 when the two-photon laser energy is scanned across its 1s A and B excitons [14]. In addition, since the first of these resonances is just above the visible spectrum at 1.65 eV [41], it holds promise for the generation of telecom-band photon pairs via SPDC.

The left inset of Fig. 3 shows our experimental setup for probing the SHG response from a monolayer of WSe_2. The nonlinear film is deposited on a quartz substrate, and both illumination and collection occur in air. A mode-locked femtosecond laser (80 MHz, 275 fs) centered at the fundamental wavelength of 1570 nm is focused through air by an infinitely-corrected objective (NA = 0.85). We fit the intensity profile of the spot at focus with a rotationally symmetric bivariate Gaussian of diameter of 1.6 μm at $1/e^2$ of its peak. We calculate the effective area of the pump at focus as $A_{SHG} = 7.854 \times 10^{-13}$ m^2 by modeling the intensity profile of the pump as a cylindrical beam with diameter $0.625 \times 1.6 = 1$ μm for energy conservation. A nonpolarizing beamsplitter is used to both reflect the pump toward the sample and collect

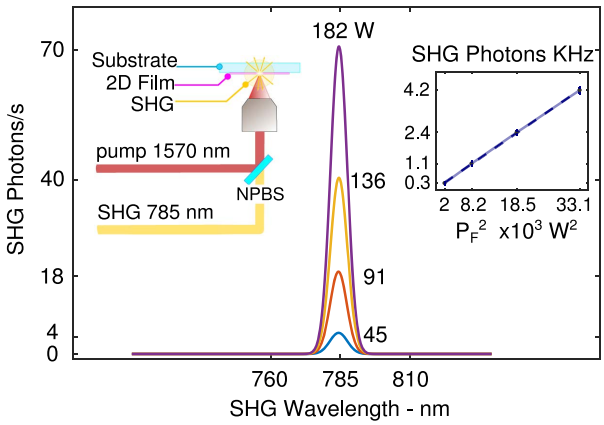

Fig. 3. Calibrated SHG spectra for different peak powers of an 80 MHz mode-locked pump centered at 1570 nm. Left inset: schematic of the experimental setup. Illumination and collection occur through the same lens (NA = 0.85), and a nonpolarizing beamsplitter (NPBS) is used to spatially separate input and output. Right inset: expected quadratic power dependence of SHG intensity.

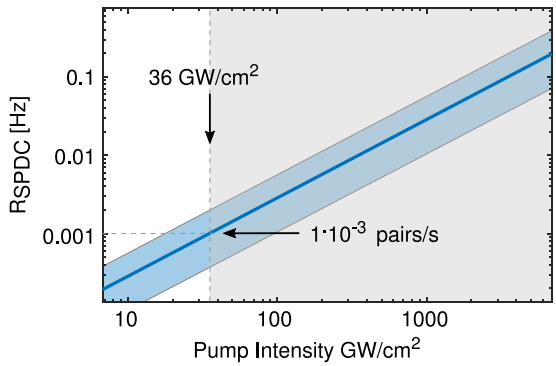

Fig. 4. While the rate of SPDC photon pairs increases linearly with pump intensity, the power damage threshold of monolayer WSe_2 (36 GW cm^{-2}) practically limits the maximum rate to 1 mHz (outside the gray shadowed area). The shaded blue area represents the uncertainty in the calculation.

the generated SHG light, which is then diffracted by a metallic grating and detected with a high-efficiency CCD array. The pump is carefully removed in the detection path by means of interference filters. Figure 3 shows spectra of the frequency-doubled light centered at half the pump wavelength, 785 nm, demonstrating that we are able to collect across the entire generation bandwidth. Intensities were calibrated to account for all collection, propagation, and detection losses and thus represent the estimated SHG photon flux that is generated by the WSe_2 monolayer and propagates in 4π sr on both sides of the sample. Spectra are presented for different peak powers corresponding to average power values ranging from 1 to 4 mW and were collected over 60 s. The blue solid line in the right inset of Fig. 3 is the ratio R_{SHG}/P_F^2, which overlaps perfectly with the line of best fit (dashed line).

In Fig. 4 we plot the predicted rate of SPDC pair generation in a monolayer of WSe_2 via Eq. (4) as a function of average pump intensity (P_P/A_{SPDC}). As an example, we consider the source to be a Coherent Ultra II commercial laser system where the pump for the SPDC experiment is generated by synchronously pumping an optical parametric oscillator (OPO) cavity with the same pulse train used in the SHG measurements ($T_F = T_P$). Frequency-resolved optical gating traces reveal values of $\Delta t_F = 275$ fs and $\Delta t_P = 235$ fs. While, theoretically, we could achieve higher and higher rates simply by increasing the pump power, in practice the damage threshold of WSe_2 will limit the achievable rate. We experimentally find this damage threshold to be 36 GWcm^{-2}, which in turn bounds the rate of SPDC-generated pairs to $R_{SPDC} = 0.001 \pm 0.0005$ pairs/s, or 1 pair every 16.7 min on average. The uncertainty, which is represented by the shaded blue area, is calculated assuming that all quantities in Eq. (4) are known with an error of 5% with the exception of R_{SHG} whose variance is estimated from the four measured data points in the right inset of Fig. 3. Yet while this rate is considerably smaller than what can be obtained in phase-matched bulk crystals [42,43] and could make the experimental observation of SPDC challenging, in the next section we identify the main contributions of noise and loss in a free-space measurement setup and show that a CAR greater than 10 could

in principle be achieved with state-of-the-art single-photon detectors. Such a measurement would set a record for photon pair generation from two-dimensional (2D) quantum confined materials as well as enable the experimental exploration of scaling laws involving excitonic resonances.

The SHG data in the right inset of Fig. 3 can also be used to calculate the effective nonlinearity $\chi^{(2)}_{\text{eff}}$ of the WSe_2 monolayer. For each of the four measured points we substitute Eq. (2) in Eq. (1) and calculate $\chi^{(2)}_{\text{eff}} = 6.63 \pm 1.92\ \text{pm/V}^{-1}$, in good agreement with previously measured values under similar optical pumping [26]. Results are obtained for illumination at 1570 nm with $\omega_{\text{SH}} = 2\pi \times 3.82 \times 10^{14}$ rad/s, $A_{\text{SHG}} = 7.85\times10^{-13}\text{m}^2$, $L = 0.7$ nm, $n_{\text{F}} = 4.0$, and $n_{\text{SH}} = 5.1$, and errors are calculated under the same assumptions detailed previously for the calculation of R_{SPDC}.

4. CAR IN COINCIDENCE MEASUREMENTS

The photon pairs generated by SPDC in atomically thick materials are emitted in the surrounding medium with a broad range of pairs of angles, and as such this interaction is best probed in free space. Such an experimental configuration has the additional advantage of decoupling the contributions of the medium and the substrate. The setup in Fig. 5 shows a single-photon Hanbury, Brown, and Twiss (HBT) interferometer where collection occurs on both sides of the nonlinear medium, light is spatially separated by a nonpolarizing beamsplitter, and is independently detected by two single-photon avalanche photodiodes. The relative time difference between detections is discretized in time bins t_{bin}, and its histogram approximates the $g^{(2)}(\tau)$ of the light source. Based on this optical arrangement we first describe all possible sources of accidental coincidences that affect the measurement of photon simultaneity in monolayer WSe_2 (see Fig. 6) and provide a simple expression for the average CAR in such a setting as a function of loss. We then consider the setup in Fig. 5 and combine measured and simulated loss terms in Section 5 to calculate the average CAR expected in a real experiment.

In addition to true coincidences resulting from a pair of photons, the HBT detectors may register accidental coincidences

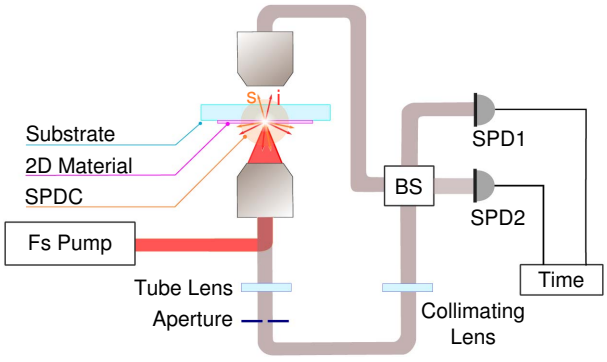

Fig. 5. Experimental setup for the measurement of the strong temporal correlation of SPDC photon pairs in monolayer WSe_2. Pump photons at 785 nm spontaneously convert into pairs of signal and idler photons around 1570 nm. The near infrared light is split at a beamsplitter, BS, and detected by single photon avalanche photodiodes for statistical analysis.

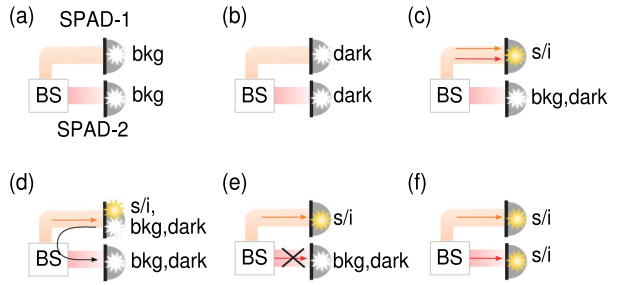

Fig. 6. Breakdown of the processes that lead to (a)–(e) accidental coincidences and (f) true coincidences: (a)–(b) simultaneous dark and background detections; (c) bunching of photon pairs at one output of the beamsplitter followed by a dark or background detection; (d) detection of breakdown flashing following any detection event; (e) linear loss causes only one photon of the pair to be detected together with noise.

due to thermal noise in the detectors R_{dark}, background radiative emission from the material statistically uncorrelated with SPDC process R_{bkg}, or breakdown flashing in the detectors R_{bf} [44]. The total rate of accidental coincidences can thus be written to account for all these effects as

$$R_{\text{AC}} = R^{\text{nn}}_{\text{dark}} + R^{\text{nn}}_{\text{bkg}} + R^{\text{nn}}_{\text{bf}} + R^{\text{ns}}_{\text{loss}} + R^{\text{ns}}_{\text{bs}}, \tag{5}$$

where a distinction is made between terms that involve two coincident *noise* detections, nn, and those involving *noise–signal* detections, ns. Note that the former are always present even if there is no generation of photon pairs. The latter, which can only occur in the presence of a mixture of signal and noise, can be further decomposed into a term that depends on the total photon loss $R^{\text{ns}}_{\text{loss}}$ and one that depends on the beamsplitter $R^{\text{ns}}_{\text{bs}}$. The former describes cases when one photon of the pair is lost and the detection of the other photon coincides with a *noise* event on the opposite arm of the interferometer. The latter, $R^{\text{ns}}_{\text{bs}}$, arises from the probabilistic bunching of the photons the beamsplitter and the simultaneous detection of a *noise* event on the opposite arm of the interferometer. If the energy band diagram of the nonlinear film is engineered so that the SPDC pump energy is sufficiently below the bandgap, spontaneous emission (i.e., fluorescence) can be neglected, $R^{\text{nn}}_{\text{bkg}} = 0$. Although spectrally broadband, breakdown flashing in actively quenched single-photon detectors can be deterministically filtered and its contribution to the accidentals neglected $R^{\text{nn}}_{\text{bf}} = 0$ [44]. Furthermore, if the rate of dark detections dominates over the rate of SPDC pairs, both $R^{\text{ns}}_{\text{loss}}$ and $R^{\text{ns}}_{\text{bs}}$ can be neglected as the number of accidentals due to *noise–noise* detections dominates over *noise–signal* ones. Under these assumptions Eq. (5) reduces to

$$R_{\text{AC}} \approx R^{\text{nn}}_{\text{dark}}. \tag{6}$$

This is the case we are concerned with, as the maximum expected rate of photon pairs calculated for a WSe_2 monolayer is five orders of magnitude smaller than typical dark count rates $R_{\text{dark}} \approx 100$ Hz.

In order to perform a statistically significant measurement of temporal correlations, the rate of true coincidences R_{TC} must exceed the accidentals R_{AC} in the time bin $t_{\text{bin}} = \tau^*$:

$$\mathrm{CAR} = \frac{R_{\mathrm{TC}}|t_{\mathrm{bin}} = \tau^*}{R_{\mathrm{AC}}|t_{\mathrm{bin}} = \tau^*} \geq \mathrm{CAR}_{\mathrm{th}} > 1. \quad (7)$$

Since signal and idler photons are emitted at the same time, R_{TC} is equal to the number of true coincidences in the bin time $t_{\mathrm{bin}} = \tau^*$. In particular, assuming that pair generation rate and loss are statistically independent process, the average rate of true coincidences is simply $R_{\mathrm{SPDC}}/\mathrm{L}_{\mathrm{T}}^2$, where R_{SPDC} is our maximum calculated rate of photon pair generation from Section 3, and L_{T} is the total loss that an SPDC photon experiences from generation to detection. With the same statistical assumptions on the thermal noise in the two detectors R_{dark}, and the assumptions that led to Eq. (6), the average rate of accidentals is $R_{\mathrm{dark}}^2 \cdot t_{\mathrm{bin}}$, which results from the product between the probability to record two simultaneous dark detections in one bin $(R_{\mathrm{dark}} \cdot t_{\mathrm{bin}})^2$ and the number of bins in one second $N_{\mathrm{bins}} = 1/t_{\mathrm{bin}}$. The average CAR thus takes the form

$$E[\mathrm{CAR}] = \frac{R_{\mathrm{SPDC}}}{\mathrm{L}_{\mathrm{T}}^2 R_{\mathrm{dark}}^2 t_{\mathrm{bin}}}, \quad (8)$$

which highlights the inverse quadratic dependence on L_{T} and thermal noise R_{dark} in the system. Once the total loss is known, it is possible to obtain a lower-bound for the $\chi^{(2)}_{\mathrm{eff}}$ required to unambiguously measure SPDC coincidences above noise in atomically thick materials in free space. Moreover, while the dark count rate cannot readily be controlled, a careful design of the experiment may lead to a reduction of the total loss. We identify three contributions to L_{T}:

$$\mathrm{L}_{\mathrm{T}} = \mathrm{L}_C \cdot \mathrm{L}_P \cdot \mathrm{L}_D, \quad (9)$$

where L_C, L_P, and L_D represent the loss, respectively, due to the mismatch between the radiation pattern of the emission and the receiving lenses (collection efficiency), the absorption in the optical path between the objective and the beamsplitter (propagation loss), and, finally, the quantum efficiency of the detectors along with the bunching at the beamsplitter (detection loss). As in Section 2, absorption loss is neglected for monolayer WSe_2. L_P and L_D may vary considerably depending on the experimental setup with a maximum quantum efficiency QE = 0.95 and lens transmissivity between 0.6 and 0.95. The use of a beamsplitter introduces a factor of two loss corresponding to the probability that both signal and idler photons bunch to one of the two output ports.

5. PAIR COLLECTION LOSS

While propagation and detection losses can be measured directly in the laboratory, the collection loss L_C for a single downconverted photon depends on its emission angle, refraction at all dielectric interfaces, and the position of the collecting optics. We analyze this numerically by modeling the pump $p(\omega_p, k_p, \theta_p, t_p)$ as a linearly polarized optical plane wave incident at time $t = t_p$ at the air/quartz interface with incidence angle $\theta = \theta_p$, angular frequency $\omega = \omega_p$, and wavevector $k = k_p$. The process of spontaneous conversion of a pump photon to signal $s(\omega_s, k_s, \theta_s, t_s)$ and idler $i(\omega_i, k_i, \theta_i, t_i)$ photons with $t_s = t_i$, is driven by the $\chi^{(2)}$ of the medium and constrained by energy and momentum conservation,

$$k_p \sin(\theta_p) = k_s \sin(\theta_s) + k_i \sin(\theta_i), \quad (10a)$$

$$\hbar\omega_p = \hbar\omega_s + \hbar\omega_i, \quad (10b)$$

where p, s, i denote pump, signal, and idler, respectively; $\hbar\omega_x$ is the photon energy; and $k_x \sin(\theta) \equiv k_{x//}$ is the component of the wavevector parallel to the planar interface between the 2D material and the surrounding dielectrics. Equation (10a) dictates the allowed departure angles θ_s and θ_i, and therefore shapes the radiation pattern of the downconverted light. Starting from an incident pump photon $p(k_p, \theta_p)$, we fix the energy of signal and idler photons symmetrically around $\hbar\omega_p/2$ and find θ_i for $0 \leq \theta_s \leq 2\pi$:

$$\theta_i = \arcsin\left(\frac{k_p \sin(\theta_p) - k_s \sin(\theta_s)}{|k_i|}\right). \quad (11)$$

In order to understand the effect of each term, we start from the simple case of $\theta_p = 0$ and degenerate SPDC in a homogeneous dielectric environment, $|k_s| = |k_i|$. When the two photons leave the interface in the same semispace, Eq. (11) has the real solution $\theta_i' = -\theta_s$, which becomes $\theta_i'' = \pi - \theta_s$ if the pairs departs in two opposite sides of the medium. Since these two events are equally likely, the joint probability distribution along a unitary circle centered at the interface is uniform and the pair emission is omnidirectional. When $\omega_s \neq \omega_i$ and $\theta_p = 0$, the idler departure angle becomes $\theta_i = \arcsin(-k_s/|k_i| \sin(\theta_s))$, which may yield complex solutions if $k_s > |k_i|$, a condition that does not depend on the photons' emission angles. Considering that there are an infinite number of equally likely solutions to Eq. (10b), this is expected to happen at random with a 50% chance. If the dielectric environment surrounding the nonlinear medium is nonhomogeneous and ω_s and ω_i are energy degenerate, it is possible that $k_s > |k_i|$, which results in complex θ_i. However, since θ_i' and θ_i'' are equally likely, there is always the corresponding case $k_s \leq |k_i|$, so the overall radiation diagram maintains its uniform shape. An angular dependence of the emission probabilities can however arise for $\theta_p \neq 0$ when $k_{p//} - k_{s//} > |k_i|$. This alters the probability to find a pair in the far field and leads to a directional radiation pattern.

We solve Eq. (11) numerically for a large number of downconversion events of a pump photon at 785 nm into pairs at around 1570 nm from a single layer of WSe_2 on a quartz substrate. We assume the material extends over an infinite plane at the boundary between two dielectrics and is rotationally symmetric so that we can restrict solutions along the plane of incidence of the pump. The presence of a higher density dielectric introduces an angle dependence in k_s and k_i, and care must be taken to select the relevant wavevector. We calculate linear Fresnel coefficients at all dielectric interfaces between the nonlinear film and the air-immersion lenses and include all losses due to absorption. Figure 7 shows the photon departure angles of signal (blue) and idler (green) photons in a normalized polar plot, discarding downconversion events that lead to evanescent waves. The distance from the origin represents the probability of finding the photon in the far field. Results are presented for two relevant moments: (a)–(b) immediately after the pair is generated and (c)–(d) after collection by a NA = 0.85 lens

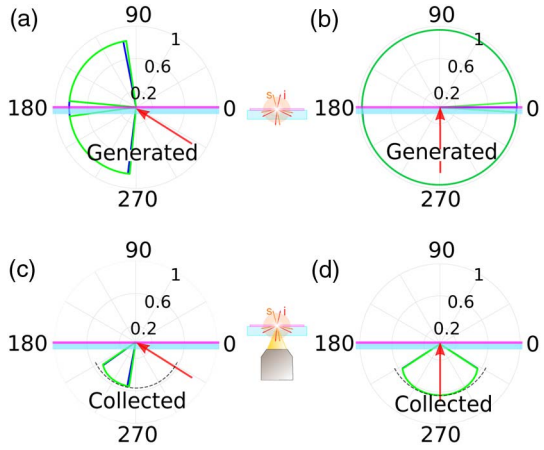

Fig. 7. Simulated radiation pattern of downconverted light from a single layer of WSe_2, which enables a calculation of the collection loss L_C. Energy and momentum conservation lead to isotropic emission of signal (blue) and idler (green) photons for normal pump incidence [red arrow in (a), (b)]. (c), (d) Single-sided photon collection further restricts the range of angles collected, reducing the probability to collect both photons.

from the air–quartz interface (c)–(d). The angular dependence of transmission coefficients shapes the radiation diagram, breaking its circular symmetry (dashed line in Fig. 7). Upon detection, photons that can be collected experience linear propagation loss while all others are lost and have a zero probability to be detected.

The first step to calculate the CAR is to estimate the rate of true coincidences, which is proportional to the probability that both photons of a pair are detected. However, since signal and idler can be emitted from both sides of the nonlinear medium, their collection probabilities may differ substantially. We therefore calculate the average pair loss L_C^2 as the inverse of the probability that both s, i are collected and detected. Figure 8 shows that the pair collection loss is minimal for normal pump

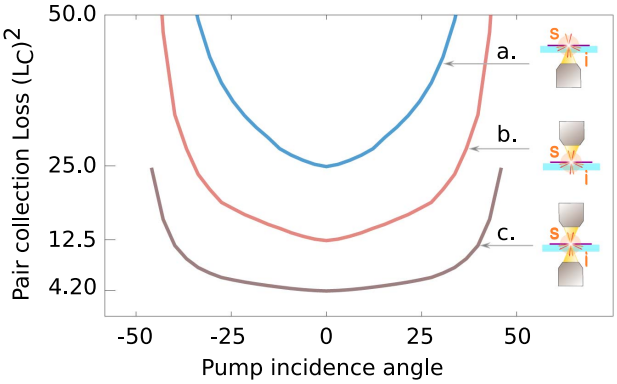

Fig. 8. Simulated collection loss of SPDC photon pairs generated in an atomically thick film on quartz with NA = 0.85. The presence of a dielectric with a higher density leads to sharper departure angles of s, i pairs and total internal reflection at the quartz–air interface, thereby increasing the pair collection loss. Normal pump incidence spreads the departure angles evenly, resulting in a higher chance to collect and detect a pair.

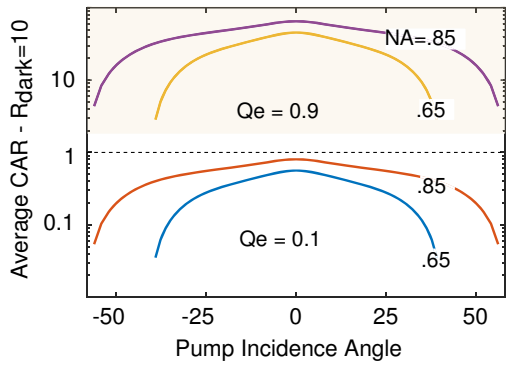

Fig. 9. Simulated CAR versus pump angle for unilateral collection of $R_{SPDC} = 0.001$ pairs/s for the best detector configurations existing to date: SPADs ($R_{dark} = 10$, QE = 0.1) and superconducting nanowire ($R_{dark} = 10$, QE = 0.9). Despite the measurement being dark-count limited, the CAR is expected to be largely above 1 for normal pump incidence and high efficiency detectors ($t_{bin} = 1$ ns).

incidence $\theta_p = 0$, which corresponds to isotropic emission of the downconverted light. Our results show that on average 1 in 4.2 pairs may be successfully collected by using two air objectives, one on each side of the interface (NA = 0.85 and transmissivity of 0.65), corresponding to a photon collection loss $L_C \approx 2$. Single-sided collection from the higher-density dielectric causes a higher pair collection loss due to the additional glass–air interface. Since the momentum is larger in the higher-density dielectric, photons generated in the higher density dielectric have sharper departures angles and a higher probability to experience total internal reflection at the quartz–air interface. This also affects the pair collection loss, making its angular dependence sharper, as visible by comparing Figs. 8(a)–8(b). Importantly, under normal pump incidence the CAR increases six-fold by collecting from the air side as opposed to the quartz side. The use of an index-matched lens is likely to dramatically reduce optical reflections and thus represents an effective way to improve the collection efficiency. However, given the weak signals expected, this would require ultrapure index-matching solutions that do not fluoresce in the spectral region of the signal and idler.

Finally, we may predict the CAR in a nonoptimized setup where collection occurs in air. Figure 9 shows the calculated CAR ($t_{bin} = 1$ ns) as a function of pump angle and lens numerical aperture for typical values of quantum efficiency of avalanche photodiodes and superconducting nanowires, respectively QE = 0.1 and QE = 0.9, and $R_{dark} = 10$ Hz. The material considered is monolayer WSe_2, for which $R_{SPDC} = 0.001$ pairs/s. With $L_C = 3.2$ and measured values of $L_P = 3.9$ and $L_D = 7.1$ we calculate $L_T = 88.8$, which corresponds to one true coincidence every 7885 generated pairs. The value of L_D implies a detection efficiency of 0.14 (or 14%) and has been extracted from the specifications of the popular ID230 InGaAs single-photon avalanche diodes (SPADs) (ID-Quantique) at 1550 nm operated at 10% efficiency. Results assume the following realistic approximations, $R_{loss}^{ns} = R_{bs}^{ns} = R_{bkg} = 0$, which is a valid assumption considering that dark count rate dominates over the photon-pair rate, and considering

the large energy separation between these latter and the material bandgap. Despite the loss, we anticipate that a measurement of photon coincidences with CAR ≥ 10 is in principle possible with single-sided collection and normal pump incidence.

6. CONCLUSIONS

The century-old discovery of SPDC has enabled a deeper understanding of light–matter interactions and has been instrumental to the development of quantum mechanics. Although SPDC has been observed in bulk and integrated structures and its scaling laws unveiled both theoretically and experimentally, measurements have been limited to interaction volumes larger than λ^3, leaving unclear how the process would scale in the presence of just a few atomic layers. In this work we considered nonlinear generation of telecom photon pairs in TMDC monolayers. We focused on WSe_2 deposited on quartz and measured the material $\chi^{(2)}$ via nonlinear spectroscopy. If multipair generation can be safely neglected, established quantum-classical relations allow us to calculate an upper bound on the rate of photon pairs while incorporating absorption loss in the medium. Results show that the pair generation efficiency is fundamentally limited by the small interaction volume and by its damage threshold and we calculate $R_{\mathrm{SPDC}} = 0.001 \pm 0.0005$ pairs/s. We then consider the measurement of photon simultaneity for free-space downconversion at the boundary between two dielectrics. Energy and momentum conservation shape the radiation pattern of the downconverted light and allow an estimation of the pair collection probability and the CAR. Pairs generated in the substrate have sharper departure angles and a higher probability to experience total internal reflection at the quartz–air interface. Moreover, normal pump incidence leads to isotropic emission of signal and idler photons and a consequent higher probability to collect a pair from free space. When all losses are accounted for, the average time between detected coincidences is on the order of tens of hours. Despite the low process efficiency, we anticipate that a CAR ≥ 10 is attainable if the thermal noise in the detectors is the only source of noise. Our findings guide the validation of established quantum-classical relations in deeply subwavelength media and provide a performance benchmark for more advanced structures based on these ultrathin materials.

Funding. School of Physics, University of Sydney; Australian Research Council (ARC) (CUDOS CE110001010); ARC Discovery Early Career Researcher Award (DECRA) (DE140100805).

Acknowledgment. This work was supported by the School of Physics of The University of Sydney, the Australian Research Council (ARC) Centre of Excellence program, and the ARC Discovery Early Career Researcher Award (DECRA).

REFERENCES

1. D. Klyshko, "Coherent photon decay in a nonlinear medium," Pis'ma Zh. Eksp. Teor. Fiz. **6**, 490–492 (1967).
2. S. E. Harris, M. Oshman, and R. Byer, "Observation of tunable optical parametric fluorescence," Phys. Rev. Lett. **18**, 732–734 (1967).
3. D. Magde, "Study in ammonium dihydrogen phosphate of spontaneous parametric interaction tunable from 4400 to 16 000 Angström," Phys. Rev. Lett. **18**, 905–907 (1967).
4. C. K. Hong and L. Mandel, "Experimental realization of a localized one-photon state," Phys. Rev. Lett. **56**, 58–60 (1986).
5. B. Zel'Dovich and D. Klyshko, "Field statistics in parametric luminescence," Sov. J. Exp. Theor. Phys. Lett. **9**, 40–42 (1969).
6. D. V. Strekalov, D. Elser, A. Aiello, U. L. Andersen, C. Marquardt, G. Leuchs, and J. U. Fu, "Quantum light from a whispering-gallery-mode disk resonator," Phys. Rev. Lett. **106**, 113901 (2011).
7. F. Michael, G. Schunk, U. F. Josef, D. Strekalov, T. Gerrits, M. J. Stevens, F. Sedlmeir, H. G. L. Schwefel, S. W. Nam, G. Leuchs, and C. Marquardt, "Highly efficient generation of single-mode photon pairs from a crystalline whispering-gallery-mode resonator source," Phys. Rev. A **91**, 023812 (2015).
8. T. Nosaka, B. K. Das, M. Fujimura, T. Suhara, and S. Member, "Cross-polarized twin photon generation device using quasi-phase matched LiNbO 3 waveguide," IEEE Photon. Technol. Lett. **18**, 124–126 (2006).
9. G. Fujii, N. Namekata, M. Motoya, S. Kurimura, and S. Inoue, "Bright narrowband source of photon pairs at optical telecommunication wavelengths using a type-II periodically poled lithium niobate waveguide," Opt. Express **15**, 12769–12776 (2007).
10. A. Valles, M. Hendrych, J. Svozilik, R. Machulka, P. Abolghasem, D. Kang, B. J. Bijlani, A. S. Helmy, and J. P. Torres, "Generation of polarization-entangled photon pairs in a Bragg reflection waveguide," Opt. Express **21**, 10841–10849 (2013).
11. P. Sarrafi, E. Y. Zhu, B. M. Holmes, D. C. Hutchings, S. Aitchison, and L. Qian, "High visibility two-photon interference of frequency-time entangled photons generated in a quasi-phase-matched AlGaAs waveguide," Opt. Lett. **39**, 5188–5191 (2014).
12. C. Autebert, N. Bruno, A. Martin, A. Lemaitre, C. Gomez Carbonell, I. Favero, G. Leo, H. ZBinden, and S. Ducci, "Integrated AlGaAs source of highly indistinguishable and energy-time entangled photons," Optica **3**, 143–146 (2016).
13. L. M. Malard, T. V. Alencar, A. P. M. Barboza, K. F. Mak, and A. M. D. Paula, "Observation of intense second harmonic generation from MoS_2 atomic crystals," Phys. Rev. B **87**, 201401 (2013).
14. G. Wang, X. Marie, I. Gerber, T. Amand, D. Lagarde, L. Bouet, M. Vidal, A. Balocchi, and B. Urbaszek, "Giant enhancement of the optical second-harmonic emission of WSe_2 monolayers by laser excitation at exciton resonances," Phys. Rev. Lett. **114**, 097403 (2015).
15. X. Yin, Z. Ye, D. A. Chenet, Y. Ye, K. O'Brien, J. C. Hone, and X. Zhang, "Edge nonlinear optics on a MoS_2 atomic monolayer," Science **344**, 488–490 (2014).
16. Y. Li, Y. Rao, K. F. Mak, Y. You, S. Wang, C. R. Dean, and T. F. Heinz, "Probing symmetry properties of few-layer MoS_2 and h-BN by optical second-harmonic generation," Nano Lett. **13**, 3329–3333 (2013).
17. R. I. Woodward, R. T. Murray, C. F. Phelan, R. E. P. de Oliveira, T. H. Runcorn, E. J. R. Kelleher, S. Li, E. C. de Oliveira, G. J. M. Fechine, G. Eda, and C. J. S. de Matos, "Characterization of the second- and third-order nonlinear optical susceptibilities of monolayer MoS_2 using multiphoton microscopy," 2D Mater. **4**, 011006 (2017).
18. C. Janisch, Y. Wang, D. Ma, N. Mehta, A. L. Elías, N. Perea-López, M. Terrones, V. Crespi, and Z. Liu, "Extraordinary second harmonic generation in tungsten disulfide monolayers," Sci. Rep. **4**, 5530 (2014).
19. M. Zhao, Z. Ye, R. Suzuki, Y. Ye, H. Zhu, J. Xiao, Y. Wang, Y. Iwasa, and X. Zhang, "Atomically phase-matched second-harmonic generation in a 2D crystal," Light Sci. Appl. **5**, e16131 (2016).
20. Q. Zhang, Y. Cheng, L.-Y. Gan, and U. Schwingenschlögl, "Repository giant valley drifts in uniaxially strained monolayer MoS_2," Phys. Rev. B **88**, 245447 (2013).
21. P. Johari and V. B. Shenoy, "Tuning the electronic properties of semiconducting transition metal dichalcogenides by applying mechanical strains," ACS Nano **6**, 5449–5456 (2012).
22. S. Horzum, H. Sahin, S. Cahangirov, P. Cudazzo, A. Rubio, T. Serin, and F. M. Peeters, "Phonon softening and direct to indirect bandgap crossover in strained single layer $MoSe_2$," Phys. Rev. B **87**, 125415 (2013).

23. B. Radisavljevic, A. Radenovic, J. Brivio, V. Giacometti, and A. Kis, "Single-layer MoS_2 transistors," Nat. Nanotechnol. **6**, 147–150 (2011).
24. A. Ramasubramaniam, D. Naveh, and E. Towe, "Tunable band gaps in bilayer transition-metal dichalcogenides," Phys. Rev. B **84**, 205325 (2011).
25. H.-J. Sung, D.-H. Choe, X. Li, Y. Dai, W. Xiong, C. Xia, D. Huang, and E. Kaxiras, "Effects of van der Waals interaction and electric field on the electronic structure of bilayer MoS_2," J. Phys. Condens. Matter **26**, 405302 (2014).
26. K. L. Seyler, J. R. Schaibley, P. Gong, P. Rivera, A. M. Jones, S. Wu, J. Yan, D. G. Mandrus, W. Yao, and X. Xu, "Electrical control of second-harmonic generation in a WSe_2 monolayer transistor," Nat. Nanotechnol. **10**, 407–411 (2015).
27. L. G. Helt, M. Liscidini, and J. E. Sipe, "How does it scale? comparing quantum and classical nonlinear optical processes in integrated devices," J. Opt. Soc. Am. B **29**, 2199–2212 (2012).
28. M. Liscidini and J. E. Sipe, "Stimulated emission tomography," Phys. Rev. Lett. **111**, 1–5 (2013).
29. L. G. Helt, M. J. Steel, and J. E. Sipe, "Spontaneous parametric down-conversion in waveguides: What's loss got to do with it?" New J. Phys. **17**, 013055 (2015).
30. L. G. Helt and M. J. Steel, "Effect of scattering loss on connections between classical and quantum processes in second-order nonlinear waveguides," Opt. Lett. **40**, 1460–1463 (2015).
31. A. Eckstein, G. Boucher, A. Lemaître, P. Filloux, I. Favero, G. Leo, J. E. Sipe, M. Liscidini, and S. Ducci, "High-resolution spectral characterization of two photon states via classical measurements," Laser Photon. Rev. **8**, L76–L80 (2014).
32. B. Fang, O. Cohen, M. Liscidini, J. E. Sipe, and V. O. Lorenz, "Fast and highly resolved capture of the joint spectral density of photon pairs," Optica **1**, 281–284 (2014).
33. I. Jizan, L. G. Helt, C. Xiong, M. J. Collins, D.-Y. Choi, C. Joon Chae, M. Liscidini, M. J. Steel, B. J. Eggleton, and A. S. Clark, "Bi-photon spectral correlation measurements from a silicon nanowire in the quantum and classical regimes," Sci. Rep. **5**, 12557 (2015).
34. D. Grassani, A. Simbula, S. Pirotta, M. Galli, M. Menotti, N. C. Harris, T. Baehr-jones, M. Hochberg, C. Galland, M. Liscidini, and D. Bajoni, "Energy correlations of photon pairs generated by a silicon microring resonator probed by stimulated four wave mixing," Sci. Rep. **6**, 8–13 (2016).
35. L. A. Rozema, C. Wang, D. H. Mahler, A. Hayat, A. M. Steinberg, J. E. Sipe, and M. Liscidini, "Characterizing an entangled-photon source with classical detectors and measurements," Optica **2**, 430–433 (2015).
36. L. Caspani, C. Xiong, B. J. Eggleton, D. Bajoni, M. Liscidini, M. Galli, R. Morandotti, and D. J. Moss, "Integrated sources of photon quantum states based on nonlinear optics," Light Sci. Appl. **6**, e17100 (2017).
37. C. K. Hong and L. Mandel, "Theory of parametric frequency downconversion of light," Phys. Rev. A **31**, 2409–2418 (1985).
38. D. C. Burnham and D. L. Weinberg, "Observation of simultaneity in parametric production of optical photon pairs," Phys. Rev. Lett. **25**, 84–87 (1970).
39. S. M. Eichfeld, C. M. Eichfeld, Y.-C. Lin, L. Hossain, and J. A. Robinson, "Rapid, non-destructive evaluation of ultrathin WSe_2 using spectroscopic ellipsometry," APL Mater. **2**, 092508 (2014).
40. R. L. Sutherland, *Handbook of Nonlinear Optics*, Optical Science and Engineering (Taylor & Francis, 2003).
41. K. He, N. Kumar, L. Zhao, Z. Wang, K. F. Mak, H. Zhao, and J. Shan, "Tightly bound excitons in monolayer WSe_2," Phys. Rev. Lett. **113**, 026803 (2014).
42. X.-l. Wang, L.-k. Chen, W. Li, H. Huang, C. Liu, C. Chen, Y. Luo, Z. Su, D. Wu, Z. Li, H. Lu, Y. Hu, X. Jiang, C. Peng, L. Li, N. Liu, Y.-A. Chen, C.-Y. Lu, and J.-W. Pan, "Experimental ten-photon entanglement," Phys. Rev. Lett. **117**, 210502 (2016).
43. L.-K. Chen, Z.-D. Li, X.-C. Yao, H. Miao, W. Li, H. Lu, Y. Xiao, Y.-B. Zhang, J. Xiao, C.-Z. Peng, L. Li, L. Nai-Le, X. Ma, C.-Y. Lu, Y.-A. Chen, and P. Jian-Wei, "Observation of ten-photon entanglement using thin BiB_3O_6 crystals," Optica **4**, 77–83 (2017).
44. L. Marini, R. Camphausen, B. J. Eggleton, and S. Palomba, "Deterministic filtering of breakdown flashing at telecom wavelengths," Appl. Phys. Lett. **111**, 213501 (2017).